

Article

Density Functional Theory Study of Methanol Steam Reforming on Pt₃Sn(111) and the Promotion Effect of a Surface Hydroxy Group

Ping He ^{1,2}, Houyu Zhu ^{2,*}, Qianyao Sun ³, Ming Li ³, Dongyuan Liu ², Rui Li ², Xiaoqing Lu ² , Wen Zhao ², Yuhua Chi ², Hao Ren ²  and Wenyue Guo ^{1,2,*}

¹ College of Science, China University of Petroleum (East China), Qingdao 266580, China; s21090045@s.upc.edu.cn

² School of Materials Science and Engineering, China University of Petroleum (East China), Qingdao 266580, China; b21140013@s.upc.edu.cn (D.L.); s21140007@s.upc.edu.cn (R.L.); luxq@upc.edu.cn (X.L.); zhaowen@upc.edu.cn (W.Z.); chiyuhua@upc.edu.cn (Y.C.); renh@upc.edu.cn (H.R.)

³ SINOPEC Dalian Research Institute of Petroleum and Petrochemicals Co., Ltd., Dalian 116045, China; sunqianyao.fshy@sinopec.com (Q.S.); liming.fshy@sinopec.com (M.L.)

* Correspondence: hyzhu@upc.edu.cn (H.Z.); wyguo@upc.edu.cn (W.G.)

Abstract: Methanol steam reforming (MSR) is studied on a Pt₃Sn surface using the density functional theory (DFT). An MSR network is mapped out, including several reaction pathways. The main pathway proposed is CH₃OH + OH → CH₃O → CH₂O → CH₂O + OH → CH₂OOH → CHOOH → COOH → COOH + OH → CO₂ + H₂O. The adsorption strengths of CH₃OH, CH₂O, CHOOH, H₂O and CO₂ are relatively weak, while other intermediates are strongly adsorbed on Pt₃Sn(111). H₂O decomposition to OH is the rate-determining step on Pt₃Sn(111). The promotion effect of the OH group is remarkable on the conversions of CH₃OH, CH₂O and *trans*-COOH. In particular, the activation barriers of the O–H bond cleavage (e.g., CH₃OH → CH₃O and *trans*-COOH → CO₂) decrease substantially by ~1 eV because of the involvement of OH. Compared with the case of MSR on Pt(111), the generation of OH from H₂O decomposition is more competitive on Pt₃Sn(111), and the presence of abundant OH facilitates the combination of CO with OH to generate COOH, which accounts for the improved CO tolerance of the PtSn alloy over pure Pt.



Citation: He, P.; Zhu, H.; Sun, Q.; Li, M.; Liu, D.; Li, R.; Lu, X.; Zhao, W.; Chi, Y.; Ren, H.; et al. Density Functional Theory Study of Methanol Steam Reforming on Pt₃Sn(111) and the Promotion Effect of a Surface Hydroxy Group. *Nanomaterials* **2024**, *14*, 318. <https://doi.org/10.3390/nano14030318>

Academic Editor: J. Karl Johnson

Received: 13 January 2024

Revised: 2 February 2024

Accepted: 2 February 2024

Published: 5 February 2024



Copyright: © 2024 by the authors. Licensee MDPI, Basel, Switzerland. This article is an open access article distributed under the terms and conditions of the Creative Commons Attribution (CC BY) license (<https://creativecommons.org/licenses/by/4.0/>).

Keywords: methanol; steam reforming; PtSn alloy; hydroxy group; density functional theory

1. Introduction

Methanol steam reforming (MSR) has been widely accepted as a candidate method of generating hydrogen for the on-board application of direct methanol fuel cells (DMFCs) [1,2]. Platinum (Pt) is generally applied as a DMFC catalyst because of its thermal stability and high catalytic activity [2–6]. However, CO molecules are primarily produced from methanol (CH₃OH) decomposition and gradually accumulate on Pt, which ultimately leads to CO poisoning and the loss of activity of Pt catalysts [7,8]. Alloying is an effective way to enhance the resistance of metal catalysts. Recently, a PtSn alloy showed promise as an efficient DMFC catalyst with considerable CH₃OH electrocatalytic rates compared to Pt [8–15], and it is reported to be active for CO oxidation [16–18]. Therefore, an in-depth study of MSR reactions on PtSn is an essential prerequisite to rationally design more efficient and stable PtSn-based catalysts for DMFC applications.

Generally, the MSR process can be summarized as the following two main reaction mechanisms based on previous experimental research studies [19–21]. The first mechanism (M1) proceeds with the direct dehydrogenation of CH₃OH and the formation of CO; then, CO is oxidized to CO₂ via the water–gas shift (WGS) reaction (H₂O + CO → H₂ + CO₂) [22,23]. The second mechanism (M2) includes the reactions of intermediates with adsorbed OH, which is generated from water decomposition (H₂O → OH + H), to yield CH₂OO, CHOOH, CHOO and, finally, H₂ and CO₂ [24–26]. From the perspective of theoretical research,

different catalyst models account for different intermediates and MSR mechanisms. Using density functional theory (DFT) calculations, Luo et al. [27] investigated MSR reactions on Co(0001) and Co(111), and their results showed that the direct decomposition of CH₂O to CO is favored rather than CH₂OOH formation, indicating the preference of the M1 mechanism. Fajin and Cordeiro [28] performed a DFT investigation on bimetallic Ni–Cu alloy surfaces and also confirmed the M1 mechanism. They found that the MSR evolves mostly through CH₃OH decomposition followed by the WGS reaction. In these studies, the surface OH group did not take part in the main reaction pathway, but it can become involved in or influence the MSR process on other metal and alloy surfaces. Lin et al. proposed that MSR reactions on Cu(111) [25,29] and PdZn(111) [26,30] follow the M2 mechanism, that is, the stepwise dehydrogenation of CH₃OH occurs first, followed by CH₂O formation; then, CH₂O combines with OH, which produces a CH₂OOH intermediate. Finally, CH₂OOH is further dehydrogenated to yield CO₂. CH₃O dehydrogenation is identified as the rate-determining step on both Cu(111) and PdZn(111) surfaces. Li et al. [31] also confirmed the M2 mechanism of the MSR on an α -MoC(100) surface using DFT calculations. The results suggest that the stepwise O–H and C–H bond scissions of CH₃OH yield CH₂O. Then, CH₂OOH is formed through the combination of CH₂O and OH, which is preferred over the decomposition path of CH₂O to CHO and H. In addition to its direct involvement in the MSR reaction pathway, the surface OH group can also exert an important influence on the MSR process. Huang et al. [32] studied CH₃OH decomposition on PdZn(111) using the DFT and found that the presence of co-adsorbed OH species would hinder C–H bond scission while significantly reducing the energy barrier of the O–H bond scission. Thus, CH₃OH preferentially undergoes O–H bond scission to form CH₃O because of the influence of OH. Although a great number of efforts have been made to determine the MSR mechanisms of various catalyst models, the detailed MSR process, as well as intermediate information, has not been unambiguously elucidated for specific new catalyst models. At present, there are no theoretical reports available to elucidate the complete MSR mechanism on a PtSn alloy surface. Furthermore, the effect of OH species on the MSR process should also be clarified.

In this work, a periodic DFT investigation is carried out to elucidate the MSR mechanism on a PtSn alloy surface. Among Pt_xSn catalysts with different Sn contents, Pt₃Sn has been proven to have the best performance for the oxidation of methanol and CO in DMFCs [17,18]. Thus, Pt₃Sn(111) is chosen as a representative PtSn alloy for DFT calculations. The adsorption structures, elementary reactions and potential energy surfaces (PESs) are illustrated for methanol decomposition and steam reformation processes, and the effect of the OH group on the catalytic mechanism is discussed in detailed.

2. Computational Methods

DFT calculations were conducted using the DMol³ program package [33–35]. Exchange and correlation effects were treated using the GGA-PW91 functional [36–38]. The DSPP method [39] was applied for Pt and Sn atoms, while C, H and O atoms were treated with an all-electron basis set. The valence electron functions were expanded into a set of numerical atomic orbitals on a double-numerical basis with polarization functions. A Fermi smearing of 0.005 Hartree and a real-space cutoff of 4.5 Å were used. Spin-polarization was applied in all calculations.

The lattice constant of the Pt₃Sn was calculated to be 4.01 Å, in good agreement with the experimental value of 4.00 Å [40]. The Pt₃Sn(111) surface was built using a p(2 × 2) unit cell with a four-layer slab, and each layer consisted of three Pt atoms and one Sn atom. The height of the vacuum region was set at 12 Å. The reciprocal space was sampled with a (5 × 5 × 1) *k*-points grid generated automatically using the Monkhorst–Pack method [41]. The uppermost two layers of the slab were relaxed with adsorbates, while two substrate layers were fixed at bulk positions.

High-symmetry sites on Pt₃Sn(111) are presented in Figure 1. The adsorption energies (E_{ads}) were calculated as follows: [42,43]

$$E_{\text{ads}} = E_{\text{adsorbate}} + E_{\text{slab}} - E_{\text{adsorbate/slab}} \quad (1)$$

where $E_{\text{adsorbate/slab}}$ is the energy of the adsorbate/slab adsorption system, and $E_{\text{adsorbate}}$ and E_{slab} are the energies of the free adsorbate and the clean slab, respectively. By this definition, stable adsorption will have a positive adsorption energy.

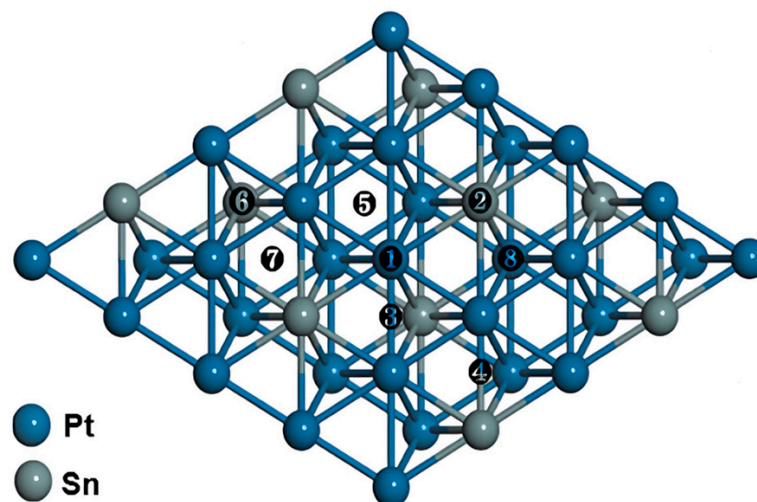


Figure 1. High-symmetry adsorption sites on Pt₃Sn(111). The labels ①~⑧ represent the top of the Pt site (T^{Pt}), the top of the Sn site (T^{Sn}), the Pt-Pt bridge site (B^{2Pt}), the Pt-Sn bridge site (B^{PtSn}), the fcc/hcp site consisting of three surface nearest-neighboring Pt atoms (F^{3Pt}/H^{3Pt}) and the fcc/hcp site consisting of one Sn and two Pt atoms (F^{2PtSn}/H^{2PtSn}), respectively.

Transition state (TS) searches were performed at the same theoretical level using the complete linear synchronous transit/quadratic synchronous transit (LST/QST) method [22–24,44]. In this method, an LST maximization was performed, followed by an energy minimization in directions conjugating to the reaction pathway to obtain an approximated TS. The approximated TS was used to perform a QST maximization, and then another conjugated gradient minimization was performed. This cycle was repeated until a stationary point was located. The convergence criterion for the TS searches was set to 0.01 hartree/Å for the root mean square of the atomic forces. The energy barrier (E_a) was determined as the energy difference between the corresponding TS and the initial state (IS), and the reaction energy (E_r) was defined as the energy difference between the final state (FS) and the IS.

3. Results and Discussion

3.1. Adsorption Structures and Energies

Figure 2 shows the most stable adsorption geometries of intermediates in MSR, and Table 1 shows the corresponding adsorption energies (E_{ads}) and geometric parameters. For clarity, the geometries and energies of the sub-stable adsorptions of the involved intermediates are presented in Figure S1 and Table S1 of the Supporting Information. In our previous study of methanol decomposition on Pt₃Sn(111) [43], several intermediates were calculated in detail, and the most stable adsorption sites along with E_{ads} can be summarized as follows CH₃OH at T^{Sn} (0.47 eV), CH₃O at T^{Sn} (1.71 eV), CH₂OH at T^{Pt} (1.94 eV), CH₂O at F^{2PtSn} (0.38 eV), CHOH at B^{2Pt} (3.14 eV), CHO at T^{Pt} (2.28 eV), COH at H^{3Pt} (4.05 eV), CO₂ at B^{PtSn} (0.11 eV), OH at B^{2Pt} (2.51 eV) and O at F^{2PtSn} (4.12 eV). In this work, we focus on the reformation process, especially the OH-involved paths. Accordingly, the reaction intermediates of MSR are described in detail below.

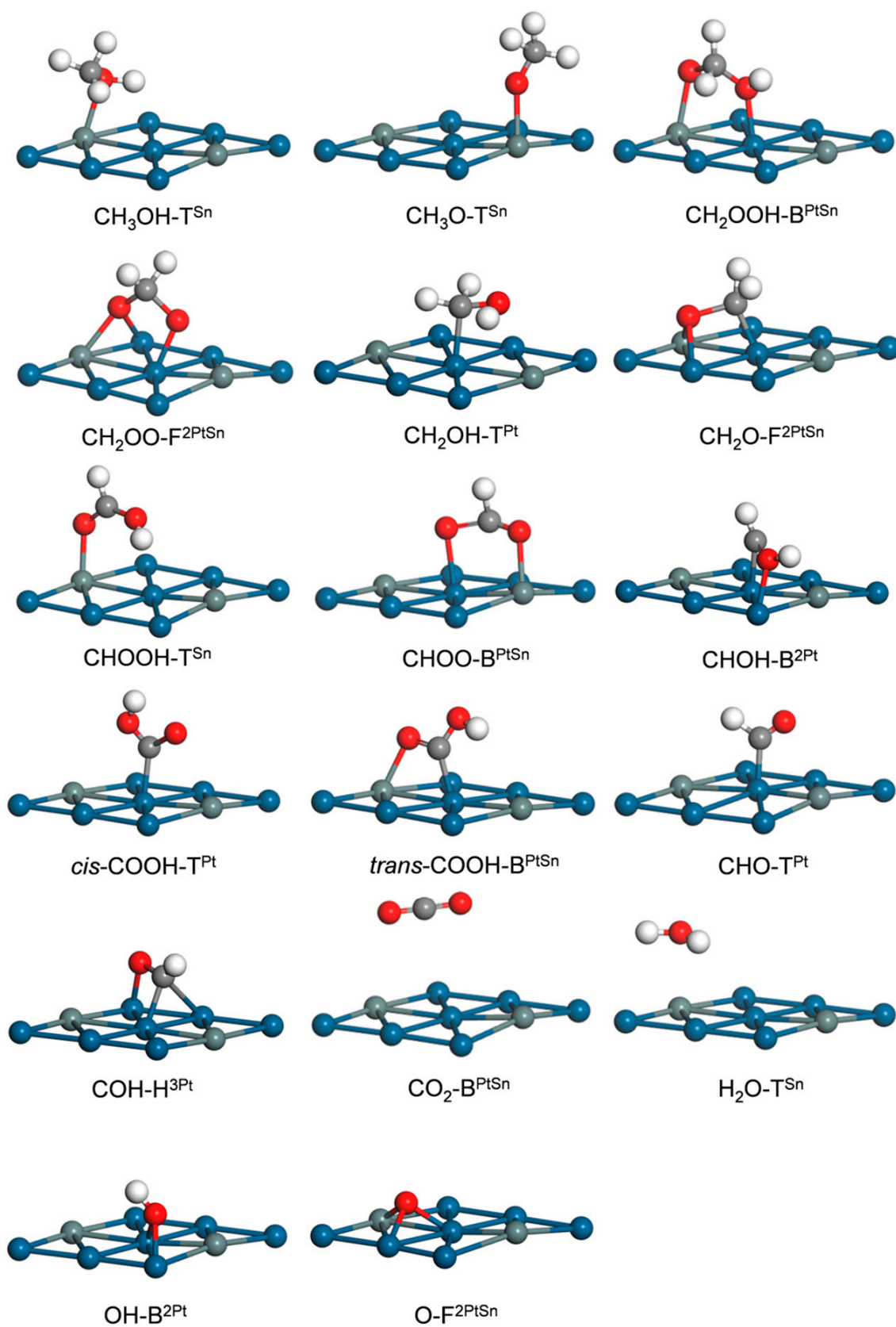


Figure 2. Stable adsorption structures of MSR intermediates on $\text{Pt}_3\text{Sn}(111)$. The C, H, O, Pt and Sn atoms are denoted as gray, white, red, blue and gray balls, respectively.

Table 1. The most stable adsorption sites, geometric parameters (in Å) and energies (in eV) for MSR intermediates on Pt₃Sn(111).

Species	Site	Mode	$d_{C/O-Pt/Sn}$	E_{ads}
CH ₃ OH	T ^{Sn}	$\eta^1(O)$	2.64	0.47
CH ₃ O	T ^{Sn}	$\eta^1(O)$	2.05	1.71
CH ₂ OOH	B ^{PtSn}	$\eta^1(O)-\eta^1(O)$	2.15, 2.31	1.89
CH ₂ OO	F ^{2PtSn}	$\eta^2(O)-\eta^1(O)$	2.09, 2.26, 2.27	3.24
CH ₂ OH	T ^{Pt}	$\eta^1(C)$	2.14	1.94
CH ₂ O	F ^{2PtSn}	$\eta^1(C)-\eta^2(O)$	2.13, 2.28, 2.43	0.38
HCOOH	T ^{Sn}	$\eta^1(O)$	2.58	0.49
CHOO	B ^{PtSn}	$\eta^1(O)-\eta^1(O)$	2.17, 2.29	2.52
CHOH	B ^{2Pt}	$\eta^2(C)$	2.09, 2.12	3.14
<i>cis</i> -COOH	T ^{Pt}	$\eta^1(C)$	2.03	2.48
<i>trans</i> -COOH	B ^{PtSn}	$\eta^1(C)-\eta^1(O)$	2.04, 2.55	2.41
CHO	T ^{Pt}	$\eta^1(C)$	2.01	2.28
COH	H ^{3Pt}	$\eta^3(C)$	2.04, 2.06, 2.11	4.05
CO ₂	B ^{PtSn}	-	-	0.11
H ₂ O	T ^{Sn}	-	-	0.01
OH	B ^{2Pt}	$\eta^2(O)$	2.23, 2.24	2.51
O	F ^{2PtSn}	$\eta^3(O)$	2.13, 2.14, 2.14	4.12

Carboxymethyl (CH₂OOH) is formed through the combination of CH₂O and an OH group and preferentially adsorbs at a bridge site via the $\eta^1(O)-\eta^1(O)$ mode, which is different from the unidentate $\eta^3(O)$ modes at the hollow sites of Cu(111) [25], PdZn(111) [26] and Co(111) [27]. The E_{ads} values of CH₂OOH are 1.89 eV (B^{PtSn}) and 1.65 (B^{2Pt}), respectively. At the B^{PtSn} site (Figure 2), two C–O bond lengths are 1.35 and 1.52 Å, and the O–Sn and O–Pt distances are 2.15 and 2.31 Å, respectively. Dioxomethylene (CH₂OO) was reported to adsorb at a bridge site in a bidentate $\eta^1(O)-\eta^1(O)$ mode on Cu(111), PdZn(111) and Co(111) surfaces [25–27]. However, we found that CH₂OO has two adsorption modes on Pt₃Sn(111) which are the $\eta^2(O)-\eta^1(O)$ mode at the F^{2PtSn} site and the $\eta^1(O)-\eta^1(O)$ mode at the B^{PtSn} site. As listed in Table 1, the $\eta^2(O)-\eta^1(O)$ mode (Figure 2) is more stable with an E_{ads} of 3.24 eV, and the two O–Pt and O–Sn distances are 2.09, 2.26 and 2.27 Å, respectively. The E_{ads} of the $\eta^1(O)-\eta^1(O)$ mode (Figure S1) was calculated to be 3.08 eV, consistent with the previous DFT result for CH₂OO adsorption via the same $\eta^1(O)-\eta^1(O)$ mode on Cu(111) [25]. For Formic acid (CHOOH), the most stable adsorption site is T^{Sn}, and the corresponding E_{ads} is 0.49 eV. The molecule plane of CHOOH is almost vertical with the OH group pointing down toward the surface (Figure 2). The two C–O bond lengths are 1.23 and 1.32 Å, respectively. The CHOOH at the T^{Pt} has a similar adsorption configuration (Figure S1) with a lower E_{ads} of 0.38 eV. The other four adsorption geometries of CHOOH at F^{2PtSn}, F^{3Pt}, H^{2PtSn} and H^{3Pt} involve molecule planes almost parallel to Pt₃Sn(111) with ~3.70 Å above the surface (Figure S1). Formate (CHOO) can adsorb at B^{2Pt} and B^{PtSn} with the $\eta^1(O)-\eta^1(O)$ mode, and the B^{PtSn} site is preferred. At the B^{PtSn} site, the molecular plane is perpendicular to the Pt₃Sn(111), with an E_{ads} of 2.52 eV; the O–Pt and O–Sn distances are 2.17 and 2.29 Å, respectively (Figure 2). At the B^{2Pt} site, the E_{ads} decreases to 2.08 eV. Carboxyl (COOH) has two isomers which are *cis*- and *trans*-COOH, respectively [25]. The *cis*-COOH can adsorb at the T^{Pt}, T^{Sn} and T^{2Pt} sites with corresponding E_{ads} values of 2.48, 1.26 and 2.37 eV, respectively. The T^{Pt} site can thus be identified as the most stable binding site for *cis*-COOH; the molecular plane is nearly perpendicular to Pt₃Sn(111), with C–Pt and two C–O bond lengths of 2.03, 1.22 and 1.37 Å, respectively (Figure 2). For *trans*-COOH, the E_{ads} values are 2.35 (T^{Pt}), 1.09 (T^{Sn}), 2.39 (T^{2Pt}) and 2.41 (T^{PtSn}) eV. The *cis* isomer binds slightly more strongly to Pt₃Sn(111) than its *trans* counterpart (2.48 vs. 2.41 eV), similar to COOH adsorption on Cu(111) [25]. CO₂ adsorbs weakly above the B^{PtSn} and B^{2Pt} sites with the same E_{ads} value of 0.11 eV. At bridge sites, this linear molecule lies almost parallel to the Pt₃Sn(111) at a distance of ~4.00 Å above the surface (Figure 2). These results are consistent with those of previous DFT studies of weak CO₂ adsorptions over Cu(111) [25],

Co(0001) [45] and Co(111) [27]. H₂O adsorbs above the T^{Sn} site via the O–Sn bond, and the two O–H axes are parallel to the Pt₃Sn(111) surface (Figure 2) with bond lengths of 0.98 Å. The binding strength of H₂O is very weak, mirrored by a low E_{ads} of 0.01 eV, which is also consistent with weak H₂O adsorption on Cu(111) [25], Co(111) [27] and Co(0001) [45]. The most stable sites and E_{ads} values for intermediates via $\eta(\text{O})$ can be summarized as followed: CH₂OOH at B^{PtSn} (1.89 eV), CH₂OO at F^{2PtSn} (3.24 eV), HCOOH at T^{Sn} (0.49 eV), CHOO at B^{PtSn} (2.52 eV), *cis*-COOH at T^{Pt} (2.48 eV), *trans*-COOH at B^{PtSn} (2.41 eV) and H₂O at T^{Sn} (0.01 eV). Taking into account the adsorption properties of other intermediates (CH₃OH, CH₂OH, CH₃O, CHOH, CH₂O, COH, CHO, etc.) [43], Sn strengthens the binding of these intermediates to the Pt₃Sn(111) surface via $\eta(\text{O})$.

3.2. Elementary Reaction Steps

The decomposition reactions of CH₃OH, CH₂OH, CH₃O, CH₂O and CHO via O–H, C–H and C–O bond scissions were calculated in our previous study [43]. We found that CH₃OH decomposition began with O–H bond scission, followed by C–H bond cleavages, that is, CH₃OH → CH₃O → CH₂O → CHO → CO. To identify the optimal MSR pathway, multiple reactions were further investigated in this work, including H₂O dissociation into OH and H and subsequent OH-involving reactions with CH₃OH and its dehydrogenated intermediates. The configurations of the involved IS, TS and FS are presented in Figures 3 and 4. Sixteen reactions (R1–R16) were considered in total with their thermodynamic and kinetic parameters.

H₂O Activation. In the IS, H₂O adsorbs weakly above the T^{Sn} site. For the reaction R1, the O–H bond is ruptured, with the H atom migrating toward the adjacent Pt atom. The O–H distance of H₂O is elongated from 0.98 Å in the IS to 1.62 Å in TS1, as shown in Figure 3. Finally, the OH binds at the B^{2Pt} site, and the H sits at the H^{3Pt} site. This reaction is exothermic by 0.47 eV, with an energy barrier of 0.97 eV. For comparison, the E_{a} of H₂O decomposition on Pt₃Sn is much lower than that on Cu(111) (1.11 eV) [25].

CH₃OH + OH. In reaction R2, CH₃OH and OH adsorb at the T^{Sn} and T^{Pt} sites in the IS, respectively, and in the FS, CH₃O and H₂O locate at the same sites as in the IS. In TS2 (Figure 3), the distance of the breaking O–H bond in CH₃OH is 1.24 Å, smaller than that in the direct dehydrogenation of CH₃OH (0.97 Å) [43]. This step is slightly exothermic by 0.04 eV, and the E_{a} is only 0.02 eV, which is 0.97 eV lower than direct methanol dehydrogenation by O–H bond cleavage at the same site of the T^{Sn} [43].

CH_xO + OH (x = 0–3). In reaction R3 of CH₃O with OH, the energy barrier is 0.84 eV with a reaction energy of –0.87 eV. In TS3, the distance of the breaking O–H bond is 1.27 Å. In reaction R4, the CH₂O fragment is weakly bound at the F^{2PtSn}, while the OH fragment stays at T^{Pt} site, yielding CH₂OOH at the B^{2Pt} site. In TS4, two fragments move to the T^{Pt} site, and the distance of the cleaved O–H bond is 2.09 Å. This step is exothermic by 0.45 eV and has an activation barrier of 0.43 eV, lower than that of 0.75 eV for CH₂O → CHO [25]. A similar process also occurs on Cu(111) [25] and PdZn(111) [26]. For reaction R5, co-adsorbed CHO at the H^{3Pt} site and OH at the T^{Sn} site are taken as the IS, and the HCOOH at the H^{3Pt} site is the FS. The distance between C and O atoms is shortened from 3.67 Å in the IS to 1.92 Å in TS5 and to 1.36 Å in the FS. This reaction has an activation barrier of 0.63 eV with an exothermicity of 0.70 eV. For reaction R6, the IS is the co-adsorption of OH at the T^{Sn} site and CO at the T^{Pt} site, and the FS is COOH at the T^{Pt} site. In TS6, the distance of the forming C–O bond is 1.91 Å. This step is exothermic by 0.25 eV, with an activation barrier of 0.39 eV.

CH₂OOH dehydrogenation. Two reaction pathways exist for CH₂OOH dehydrogenation. The first is C–H bond scission (R7, CH₂OOH → CHOOH + H), producing a CHOOH fragment above the B^{PtSn} site with H at the H^{3Pt} site. For TS7 (Figure 3), the C–H distance of the breaking C–H bond is 1.53 Å, which stretches from 1.11 Å in the IS to 3.95 Å in the FS. This reaction has an activation barrier of 0.40 eV with a reaction energy of –0.74 eV. The second is O–H bond scission (R8, CH₂OOH → CH₂OO + H), which starts with the CH₂OOH at the B^{2Pt} site and ends with a co-adsorbed CH₂OO fragment at the B^{2Pt} site and

H at the T^{Pt} site. In TS8 (Figure 3), the O–H distance of the breaking O–H bond is 1.49 Å. This reaction has a higher activation barrier of 1.64 eV and is endothermic by 0.91 eV. Based on thermodynamic and kinetic viewpoints, CH_2OOH dehydrogenation on $\text{Pt}_3\text{Sn}(111)$ tends to yield CHOOH rather than CH_2OO , that is, the C–H bond scission of reaction R7 is more competitive than the O–H bond scission of reaction R8.

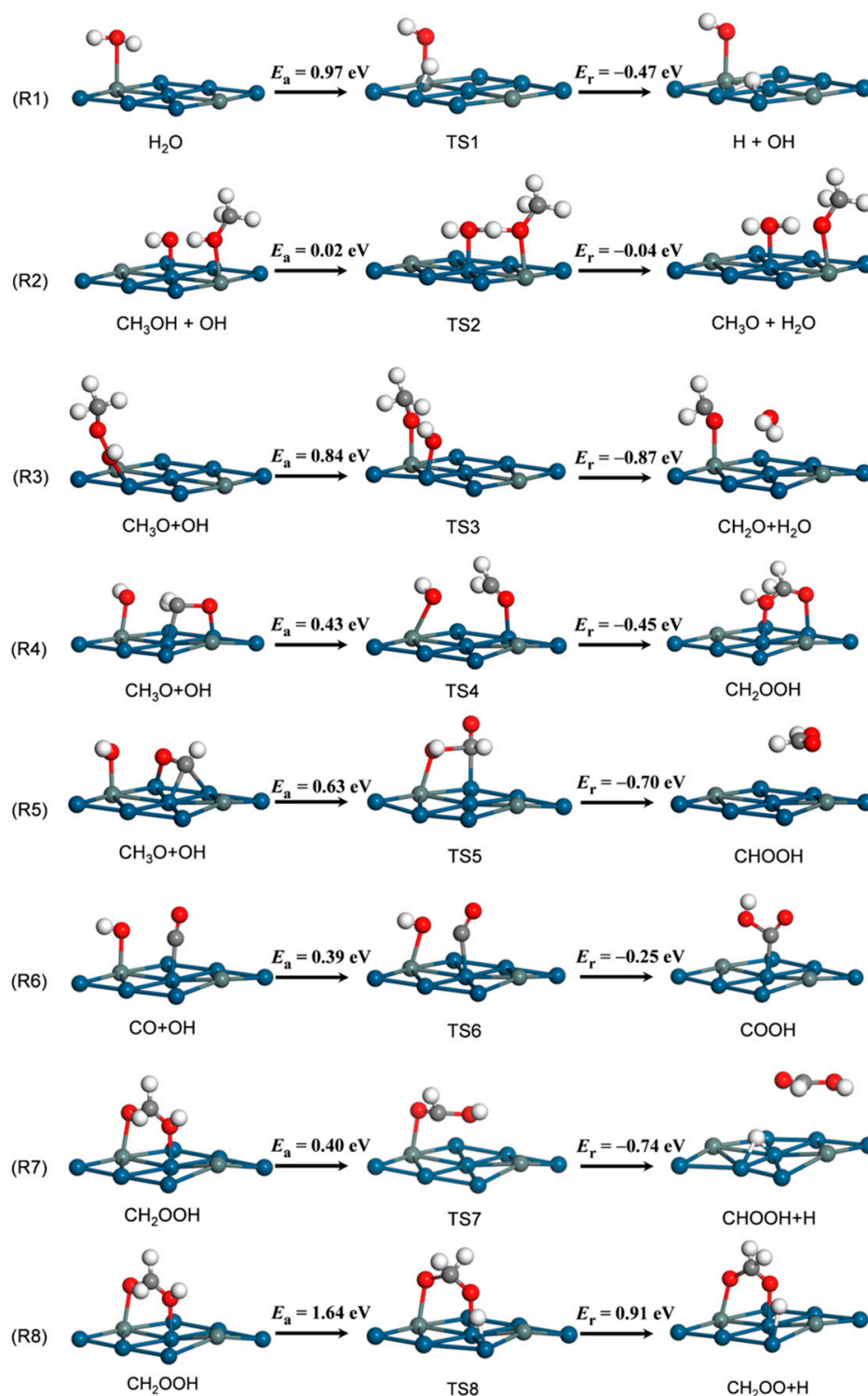


Figure 3. MSR reactions involving OH (R1–R8) on $\text{Pt}_3\text{Sn}(111)$. Parameters follow the same notation as in Figure 2.

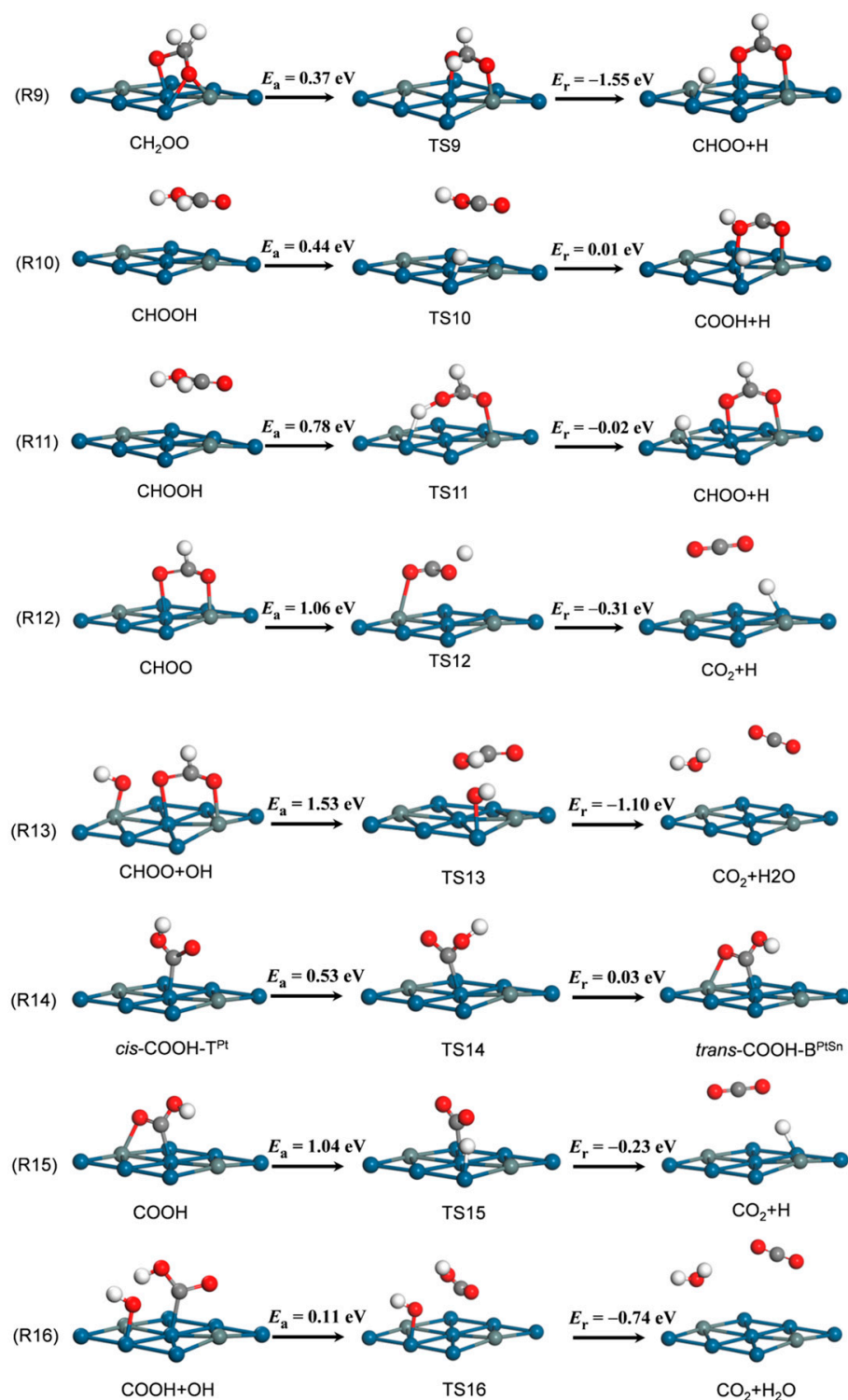


Figure 4. The MSR reactions involving OH (R9–R16) on Pt₃Sn(111). Parameters follow the same notation as in Figure 2.

CH₂OO and CHOOH dehydrogenation. CH₂OO dehydrogenation, denoted as reaction R9, yields bidentate CHOO binding at the B^{PtSn} site and H at the T^{Pt} site (Figure 4). This step has a low activation barrier of 0.37 eV and a high exothermicity of 1.55 eV. For TS9, H moves down and locates above the B^{2Pt} site, while CHOO remains at the B^{PtSn} site; the C–H distance of the breaking C–H bond is 1.11 Å. CHOOH dehydrogenation includes C–H bond scission (reaction R10) and O–H bond cleavage (reaction R11). The C–H bond cleav-

age of CHOOH yields a B^{PtSn} -site-adsorbed COOH fragment and a T^{Pt} -site-adsorbed H atom (Figure 4). This reaction involves an energy barrier of 0.44 eV and an endothermicity of 0.01 eV. For TS10, the breaking C–H bond is elongated to 2.07 Å. The O–H bond cleavage of CHOOH is slightly exothermic by 0.02 eV, and the activation barrier is 0.78 eV. For TS11, the O–H bond is elongated by 1.35 Å, and the leaving H adsorbs at the B^{2Pt} site. In the FS, CHOO binds to the $Pt_3Sn(111)$ surface in a bidentate configuration, and the detached H locates at the T^{Pt} site.

CHOO and COOH dehydrogenation. The CHOO is produced from CH_2OO dehydrogenation or CHOOH dehydrogenation via the O–H bond cleavage. The further dehydrogenation of CHOO generates CO_2 and an H atom, which is denoted as reaction R12 (Figure 4). In TS12, the C–H distance of the breaking C–H bond is 2.40 Å. After the C–H bond scission, the detached H atom adsorbs at the T^{Pt} site, while the CO_2 adsorbs above the B^{PtSn} site. This reaction is exothermic by 0.31 eV, and the activation barrier is 1.06 eV. The dehydrogenation process of CHOO could also be accomplished with assistance from an adsorbed OH group (reaction R13). This step starts with co-adsorbed CHOO at the B^{PtSn} site and OH at the T^{Pt} site and ends with weakly bonded CO_2 and H_2O on the surface. The activation barrier of this step is 1.53 eV, and the reaction energy is -1.10 eV. Compared with the direct dehydrogenation of CHOO (R12), the OH-assisted reaction of CHOO with OH to H_2O and CO_2 (R13) has a relatively higher energy barrier, suggesting that R12 is more favorable than R13. The isomerization of *cis*-COOH to form *trans*-COOH (R14) is necessary for COOH dehydrogenation because the O–H bond of the adsorbed COOH points away from the surface in the *cis*-mode but swings toward the surface in the *trans*-mode, which is helpful for O–H bond activation. This isomerization step involves an energy barrier of 0.53 eV. Subsequently, CO_2 is produced by removing the H atom from *trans*-COOH (R15), which accounts for an activation barrier of 1.04 eV and a reaction energy of -0.23 eV. For TS15, the O–H distance of the breaking O–H bond is 1.38 Å, and the CO_2 is above the B^{PtSn} site and an H atom locates at the T^{Pt} site. Similar to CHOO, *trans*-COOH can also react with OH to generate H_2O and CO_2 (R16). This step starts with co-adsorbed *trans*-COOH at the T^{Pt} site and OH at the B^{PtSn} site and ends with CO_2 above the B^{PtSn} site and H_2O above the T^{Pt} site. This OH-assisted step is exothermic by 0.74 eV, with a lower activation barrier of 0.11 eV.

3.3. MSR Mechanisms

Based on the calculated results, the potential energy surfaces of MSR on $Pt_3Sn(111)$ are presented in Figure 5. CH_3OH decomposition with the assistance of OH to form $CH_3O + H_2O$ and CH_3OH dehydrogenation via O–H bond scission to form $CH_3O + H$ involve activation barriers of 0.02 and 1.01 eV, respectively. Compared with the direct dehydrogenation of CH_3OH to CH_3O on $Pt_3Sn(111)$, the involvement of the OH group greatly promotes this dehydrogenation step. For the intermediate CH_3O , however, the OH group is not helpful for C–H bond cleavage because the direct dehydrogenation of CH_3O to CH_2O only needs to overcome an activation barrier of 0.42 eV compared with the case of $CH_3O + OH \rightarrow CH_2O + H_2O$ ($E_a = 0.84$ eV). For the intermediate CH_2O , the transition state of the C–H bond activation with the participation of the OH group was not found in spite of an elaborate search. CH_2O has two competitive paths: the direct dehydrogenation, $CH_2O \rightarrow CHO$ ($E_a = 0.75$ eV), and a combination with the OH group, $CH_2O + OH \rightarrow CH_2OOH$ ($E_a = 0.43$ eV). Therefore, the combination of CH_2O with OH is more favorable. The further dehydrogenation of the newly formed CH_2OOH has two possibilities, which are O–H and C–H bond activations. We found that the C–H bond scission of $CH_2OOH \rightarrow CHOOH + H$ ($E_a = 0.40$ eV) is more competitive than the O–H bond cleavage of $CH_2OOH \rightarrow CH_2OO + H$ ($E_a = 1.64$ eV). Similar to CH_2OOH , the intermediate CHOOH also tends to break the C–H bond ($E_a = 0.44$ eV) rather than the O–H bond ($E_a = 0.78$ eV). CHOOH dehydrogenation yields *cis*-COOH, followed by an isomerization step toward *trans*-COOH. Compared with *cis*-COOH, the adsorption geometry of *trans*-COOH is favored for O–H bond activation: *trans*-COOH $\rightarrow CO_2 + H$ ($E_a = 1.04$ eV). The

participation of the OH group substantially reduces the dehydrogenation barrier of *trans*-COOH via $\text{trans-COOH} + \text{OH} \rightarrow \text{CO}_2 + \text{H}_2\text{O}$ ($E_a = 0.11$ eV), indicating the promotion effect of the OH group.

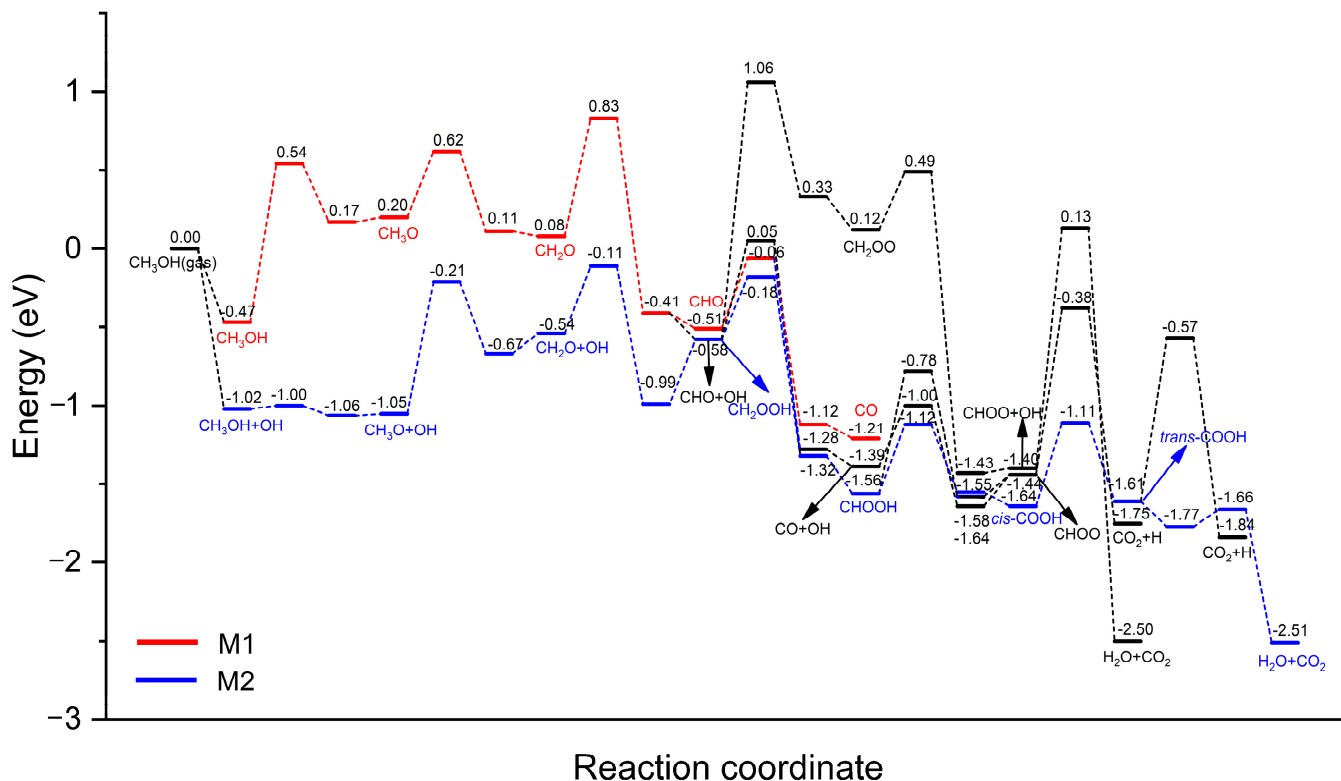


Figure 5. Potential energy surface (PES) of MSR on Pt₃Sn(111). The detailed reaction pathways of the M1 and M2 mechanisms are shown in red and blue colors, respectively. Data on the direct decomposition of methanol ($\text{CH}_3\text{OH} \rightarrow \text{CH}_3\text{O} \rightarrow \text{CH}_2\text{O} \rightarrow \text{CHO} \rightarrow \text{CO}$) were taken from our precious work [43].

Figure 6 summarizes the MSR reaction network based on the direct decomposition of methanol in our previous work [43] and the results calculated in this study. The most favorable pathway follows the M2 mechanism, in which important intermediates were identified as follows:



H₂ production originates from H₂O decomposition and the dehydrogenation of important intermediates (CH₃O, CH₂OOH and CHOOH). The promotion effect of the surface OH group on the conversions of CH₃OH, CH₂O and *trans*-COOH is remarkable. In particular, the energy barriers of the O–H bond activation (e.g., CH₃OH → CH₃O and *trans*-COOH → CO₂) decrease substantially by ~1 eV due to the involvement of the surface OH group, while OH fails to facilitate C–H bond activation. The above results are consistent with previous DFT calculations of CH₃OH decomposition by Huang et al. [32] in which the presence of a surface OH group on PdZn(111) impeded the C–H bond scission of CH₃OH but substantially decreased the O–H bond-activation barrier. For comparison,

Jin et al. [46] found that the OH group on Pt(111) could also be beneficial to MSR reactions, such as $\text{CH}_3\text{OH} \rightarrow \text{CH}_3\text{O}$ and $\text{CH}_2\text{O} + \text{OH} \rightarrow \text{CH}_2\text{OOH}$. However, it is relatively difficult to dissociate water and generate the OH group on Pt(111) compared with the direct dehydrogenation of CH_3OH . The OH group is only available when the difference in the energy barrier between H_2O decomposition and CH_3OH dehydrogenation is comparable. Thus, the MSR process on Pt(111) still follows the M1 mechanism, which is stepwise CH_3OH decomposition to CO followed by WGS reactions: $\text{CH}_3\text{OH} \rightarrow \text{CH}_2\text{OH} \rightarrow \text{CHOH} \rightarrow \text{CHO} \rightarrow \text{CO} \rightarrow \text{CO} + \text{OH} \rightarrow \text{COOH}$. In this study, the $\text{Pt}_3\text{Sn}(111)$ surface reduced the difference in the E_a between $\text{H}_2\text{O} \rightarrow \text{H} + \text{OH}$ ($E_a = 0.97$ eV) and $\text{CH}_3\text{OH} \rightarrow \text{CH}_3\text{O} + \text{H}$ ($E_a = 1.01$ eV)/ $\text{CH}_3\text{OH} \rightarrow \text{CH}_2\text{OH} + \text{H}$ ($E_a = 1.09$ eV). The relatively lower E_a of H_2O decomposition indicates the availability of the OH group, which facilitates the MSR process. The initial H_2O decomposition to the OH group involves the highest activation barrier of 0.97 eV through the main reaction pathway. Thus, H_2O decomposition could be identified as the rate-determining step for MSR on $\text{Pt}_3\text{Sn}(111)$ rather than the commonly accepted C–H bond-cleavage steps such as $\text{CH}_3\text{OH} \rightarrow \text{CH}_2\text{OH}$ on Pt(111) [46] and $\text{CH}_3\text{O} \rightarrow \text{CH}_2\text{O}$ on both Cu(111) [25] and PdZn(111) [26]. Compared with the dehydrogenation reactions of CH_3OH , the initial $\text{H}_2\text{O} \rightarrow \text{OH}$ step involves relatively higher selectivity on Pt_3Sn , which accounts for the improved CO tolerance of PtSn alloys over pure Pt.

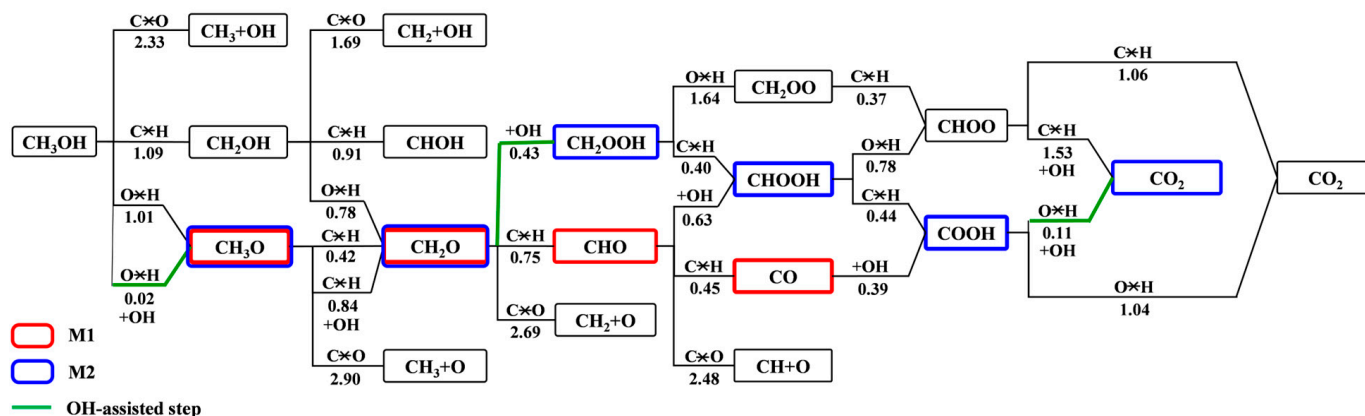


Figure 6. Proposed detailed MSR pathways on $\text{Pt}_3\text{Sn}(111)$. The M1 and M2 mechanisms are denoted by red and blue boxes, respectively. The OH-assisted steps are marked with green lines. The generated H and H_2O are omitted for clarity.

4. Conclusions

DFT calculations were performed to investigate possible intermediates and MSR reaction pathways on $\text{Pt}_3\text{Sn}(111)$. The MSR network was mapped out. The most favorable pathway was identified as follows: $\text{CH}_3\text{OH} + \text{OH} \rightarrow \text{CH}_3\text{O} \rightarrow \text{CH}_2\text{O} \rightarrow \text{CH}_2\text{O} + \text{OH} \rightarrow \text{CH}_2\text{OOH} \rightarrow \text{CHOOH} \rightarrow \text{COOH} \rightarrow \text{COOH} + \text{OH} \rightarrow \text{CO}_2 + \text{H}_2\text{O}$. Along this main reaction pathway, the adsorption strengths of CH_3OH , CH_2O , CHOOH , H_2O and CO_2 are relatively weak ($E_{\text{ads}} < 0.5$ eV), while other intermediates are strongly adsorbed at the T^{Sn} site for CH_3O ($E_{\text{ads}} = 1.71$ eV), at the T^{Pt} site for *cis*- COOH ($E_{\text{ads}} = 2.48$ eV) and at the B^{PtSn} site for CH_2OOH ($E_{\text{ads}} = 1.89$ eV) and *trans*- COOH ($E_{\text{ads}} = 2.41$ eV). H_2 production originates from H_2O decomposition and the dehydrogenation of important intermediates (CH_3O , CH_2OOH and CHOOH). H_2O decomposition into OH involves an activation barrier of 0.97 eV and was identified as the rate-determining step for the MSR process on $\text{Pt}_3\text{Sn}(111)$. The promotion effect of the surface OH group on the conversions of CH_3OH , CH_2O and *trans*- COOH is remarkable. In particular, the energy barriers of the O–H bond activation (e.g., $\text{CH}_3\text{OH} \rightarrow \text{CH}_3\text{O}$ and *trans*- $\text{COOH} \rightarrow \text{CO}_2$) decrease substantially by ~ 1 eV due to the involvement of the surface OH group. Compared with the case on Pt(111), the formation of a surface OH group from H_2O decomposition is more competitive on $\text{Pt}_3\text{Sn}(111)$, and the

presence of abundant OH facilitates the combination of CO with OH to generate COOH, which accounts for the improved CO tolerance of PtSn alloys over pure Pt.

Supplementary Materials: The following supporting information can be downloaded at: <https://www.mdpi.com/article/10.3390/nano14030318/s1>, Figure S1. The other adsorption configurations of reaction intermediates along reaction pathway of Methanol Steam Reforming (MSR) to CO₂ on Pt₃Sn(111); Table S1. Sub-stable Adsorption Sites, Energies (in eV) and Structural Parameters (in Angstroms) for Intermediates Involved in MSR on Pt₃Sn(111).

Author Contributions: Conceptualization, H.Z. and X.L.; Methodology, D.L., Y.C. and H.R.; Software, H.Z., W.Z. and W.G.; Validation, R.L.; Formal analysis, D.L. and R.L.; Investigation, P.H.; Resources, H.Z., Q.S., M.L., X.L. and H.R.; Data curation, W.Z. and H.R.; Writing—original draft, P.H.; Writing—review & editing, H.Z.; Visualization, Y.C.; Supervision, H.Z. and W.G.; Project administration, W.G.; Funding acquisition, Q.S., M.L. and W.G. All authors have read and agreed to the published version of the manuscript.

Funding: This work was funded by the National Key Research and Development Program of China (2019YFA0708703), the National Natural Science Foundation of China (21776315 and 12104513), the Taishan Scholars Program of Shandong Province (tsqn201909071) and the Shandong Provincial Natural Science Foundation of China (ZR2020QA050 and ZR2023MB034).

Data Availability Statement: Data are contained within the article.

Conflicts of Interest: Authors Qianyao Sun and Ming Li were employed by the company SINOPEC Dalian Research Institute of Petroleum and Petrochemicals Co., Ltd. The remaining authors declare that the research was conducted in the absence of any commercial or financial relationships that could be construed as a potential conflict of interest.

References

1. Palo, D.R.; Dagle, R.A.; Holladay, J.D. Methanol Steam Reforming for Hydrogen Production. *Chem. Rev.* **2007**, *107*, 3992–4021. [[CrossRef](#)] [[PubMed](#)]
2. Sá, S.; Silva, H.; Brandão, L.; Sousa, J.M.; Mendes, A. Catalysts for Methanol Steam Reforming—A Review. *Appl. Catal. B Environ.* **2010**, *99*, 43–57. [[CrossRef](#)]
3. Song, S.Y.; Wang, X.; Li, S.L.; Wang, Z.; Zhu, Q.; Zhang, H.J. Pt Nanohelices with Highly Ordered Horizontal Pore Channels as Enhanced Photothermal Materials. *Chem. Sci.* **2015**, *6*, 6420–6424. [[CrossRef](#)] [[PubMed](#)]
4. Antolini, E. Formation of Carbon-Supported PtM Alloys for Low Temperature Fuel Cells: A Review. *Mater. Chem. Phys.* **2003**, *78*, 563–573. [[CrossRef](#)]
5. Zhao, L.M.; Wang, S.P.; Ding, Q.Y.; Xu, W.B.; Sang, P.P.; Chi, Y.H.; Lu, X.Q.; Guo, W.Y. The Oxidation of Methanol on PtRu(111): A Periodic Density Functional Theory Investigation. *J. Phys. Chem. C* **2015**, *119*, 20389–20400. [[CrossRef](#)]
6. Wang, X.; Zhang, Y.B.; Song, S.Y.; Yang, X.G.; Wang, Z.; Jin, R.C.; Zhang, H.J. L-Arginine-Triggered Self-Assembly of CeO₂ Nanosheaths on Palladium Nanoparticles in Water. *Angew. Chem. Int. Ed.* **2016**, *55*, 4542–4546. [[CrossRef](#)]
7. Greeley, J.; Mavrikakis, M. A First-Principles Study of Methanol Decomposition on Pt(111). *J. Am. Chem. Soc.* **2002**, *124*, 7193–7201. [[CrossRef](#)]
8. Hoseini, S.J.; Barzegar, Z.; Bahrami, M.; Roushani, M.; Rashidi, M. Organometallic Precursor Route for the Fabrication of PtSn Bimetallic Nanotubes and Pt₃Sn/Reduced-graphene Oxide Nanohybrid Thin Films at Oilwater Interface and Study of Their Electrocatalytic Activity in Methanol Oxidation. *J. Organomet. Chem.* **2014**, *769*, 1–6. [[CrossRef](#)]
9. Antolini, E.; Gonzalez, E.R. Effect of Synthesis Method and Structural Characteristics of Pt–Sn Fuel Cell Catalysts on the Electro-oxidation of CH₃OH and CH₃CH₂OH in Acid Medium. *Catal. Today* **2011**, *160*, 28–38. [[CrossRef](#)]
10. Ishikawa, Y.; Liao, M.S.; Cabrera, C.R. Oxidation of Methanol on Platinum, Ruthenium and Mixed Pt–M Metals (M = Ru, Sn): A Theoretical Study. *Surf. Sci.* **2000**, *463*, 66–80. [[CrossRef](#)]
11. Honma, I.; Toda, T. Temperature Dependence of Kinetics of Methanol Electro-oxidation on PtSn Alloys. *J. Electrochem. Soc.* **2003**, *150*, A1689–A1692. [[CrossRef](#)]
12. Zhou, W.J.; Zhou, B.; Li, W.Z.; Zhou, Z.H.; Song, S.Q.; Sun, G.Q.; Xin, Q.; Douvartzides, S.; Goula, M.; Tsiakaras, P. Performance Comparison of Low-Temperature Direct Alcohol Fuel Cells with Different Anode Catalysts. *J. Power Sources* **2004**, *126*, 16–22. [[CrossRef](#)]
13. Kim, M.; Pratt, S.J.; King, D.A. In Situ Characterization of the Surface Reaction between Chemisorbed Ammonia and Oxygen on Pt(100). *J. Am. Chem. Soc.* **2000**, *122*, 2409–2410. [[CrossRef](#)]
14. Alcalá, R.; Shabaker, J.W.; Huber, G.W.; Marco, A.; Sanchez-Castillo, M.A.; Dumesic, J.A. Experimental and DFT Studies of the Conversion of Ethanol and Acetic Acid on PtSn-Based Catalysts. *J. Phys. Chem. B* **2005**, *109*, 2074–2085. [[CrossRef](#)] [[PubMed](#)]

15. Radael, G.N.; Oliveira, G.G.; Pontes, R.M. A DFT study of ethanol interaction with the bimetallic clusters of PtSn and its implications on reactivity. *J. Mol. Graph. Model.* **2023**, *125*, 108621. [[CrossRef](#)] [[PubMed](#)]
16. García-Rodríguez, S.; Peña, M.A.; Fierro, J.L.G.; Rojas, S. Controlled Synthesis of Carbon-Supported Pt₃Sn by Impregnation-reduction and Performance on the Electrooxidation of CO and Ethanol. *J. Power Sources* **2010**, *195*, 5564–5572. [[CrossRef](#)]
17. Colmati, F.; Antolini, E.; Gonzalez, E.R. Pt–Sn/C Electrocatalysts for Methanol Oxidation Synthesized by Reduction with Formic Acid. *Electrochim. Acta* **2005**, *50*, 5496–5503. [[CrossRef](#)]
18. Lim, D.H.; Choi, D.H.; Lee, W.D.; Lee, H.I. A New Synthesis of a Highly Dispersed and CO Tolerant PtSn/C Electrocatalyst for Low-Temperature Fuel Cell; its Electrocatalytic Activity and Long-term Durability. *Appl. Catal. B* **2009**, *89*, 484–493. [[CrossRef](#)]
19. Cai, F.F.; Jessica, J.I.; Fu, Y.; Kong, W.; Zhang, J.; Sun, Y. Low-temperature Hydrogen Production from Methanol Steam Reforming on Zn-modified Pt/MoC Catalysts. *Appl. Catal. B Environ.* **2020**, *264*, 118500. [[CrossRef](#)]
20. Conant, T.; Karim, A.; Lebarbier, V.; Wang, Y.; Girgsdies, F.; Schlögl, R.; Datye, A. Stability of Bimetallic Pd–Zn Catalysts for the Steam Reforming of Methanol. *J. Catal.* **2008**, *257*, 64–70. [[CrossRef](#)]
21. Liu, Z.; Guo, B. Microwave Heated Polyol Synthesis of Carbon-supported PtSn Nanoparticles for Methanol Electrooxidation. *Electrochem. Commun.* **2006**, *8*, 83–90. [[CrossRef](#)]
22. Wang, K.; Gasteiger, H.A.; Markovic, N.M.; Ross, P.N., Jr. On the Reaction Pathway for Methanol and Carbon Monoxide Electrooxidation on Pt–Sn Alloy versus Pt–Ru Alloy Surfaces. *Electrochim. Acta* **1996**, *41*, 2587–2593. [[CrossRef](#)]
23. Trimm, D.L.; Önsan, Z.I. On Board Fuel Conversion for Hydrogen-fuel-cell-driven Vehicles. *Catal. Rev.* **2001**, *43*, 31–84. [[CrossRef](#)]
24. Takezawa, N.; Iwasa, N. Steam Reforming and Dehydrogenation of Methanol: Difference in the Catalytic Functions of Copper and Group VIII Metals. *Catal. Today* **1997**, *36*, 45–56. [[CrossRef](#)]
25. Lin, S.; Johnson, R.S.; Smith, G.K.; Xie, D.; Guo, H. Pathways for Methanol Steam Reforming involving Adsorbed Formaldehyde and Hydroxyl Intermediates on Cu(111): Density Functional Theory Studies. *Phys. Chem. Chem. Phys.* **2011**, *13*, 9622–9631. [[CrossRef](#)] [[PubMed](#)]
26. Lin, S.; Xie, D.Q.; Guo, H. Pathways of Methanol Steam Reforming on PdZn and Comparison with Cu. *J. Phys. Chem. C* **2011**, *115*, 20583–20589. [[CrossRef](#)]
27. Luo, W.J.; Asthagiri, A. Density Functional Theory Study of Methanol Steam Reforming on Co(0001) and Co(111) Surfaces. *J. Phys. Chem. C* **2014**, *118*, 15274–15285. [[CrossRef](#)]
28. Fajín, J.L.C.; Cordeiro, M.N.D.S. Insights into the Mechanism of Methanol Steam Reforming for Hydrogen Production over Ni–Cu-Based Catalysts. *ACS Catal.* **2022**, *12*, 512–526. [[CrossRef](#)]
29. Lin, S.; Xie, D.Q.; Guo, H. Methyl Formate Pathway in Methanol Steam Reforming on Copper: Density Functional Calculations. *ACS Catal.* **2011**, *1*, 1263–1271. [[CrossRef](#)]
30. Lin, S.; Xie, D.Q.; Guo, H. First-principles Study of the Methyl Formate Pathway of Methanol Steam Reforming on PdZn(111) with Comparison to Cu(111). *J. Mol. Catal. A Chem.* **2012**, *356*, 165–170. [[CrossRef](#)]
31. Li, J.; Wan, Q.; Lin, G.Z.; Lin, S. DFT Study on the Catalytic Role of α -MoC(100) in Methanol Steam Reforming. *J. Chem. Phys.* **2022**, *35*, 639–646. [[CrossRef](#)]
32. Huang, Y.; He, X.; Chen, Z.X. Density Functional Study of Methanol Decomposition on Clean and O or OH Adsorbed PdZn(111). *J. Chem. Phys.* **2013**, *138*, 184701. [[CrossRef](#)]
33. Delley, B. An All-electron Numerical Method for Solving the Local Density Functional for Polyatomic Molecules. *J. Chem. Phys.* **1990**, *92*, 508–517. [[CrossRef](#)]
34. Delley, B. Fast Calculation of Electrostatics in Crystals and Large Molecules. *J. Chem. Phys.* **1996**, *100*, 6107–6110. [[CrossRef](#)]
35. Delley, B. From Molecules to Solids with the DMol³ Approach. *J. Chem. Phys.* **2000**, *113*, 7756–7764. [[CrossRef](#)]
36. Perdew, J.P. Density Functional Approximation for the Correlation Energy of the Inhomogeneous Electron Gas. *Phys. Rev. B Condens. Matter Mater. Phys.* **1986**, *33*, 8822–8824. [[CrossRef](#)] [[PubMed](#)]
37. Perdew, J.P.; Wang, Y. Accurate and Simple Analytic Representation of the Electron–Gas Correlation Energy. *Phys. Rev. B Condens. Matter Mater. Phys.* **1992**, *45*, 13244–13249. [[CrossRef](#)]
38. Perdew, J.P.; Burke, K.; Ernzerhof, M. Generalized Gradient Approximation Made Simple. *Phys. Rev. Lett.* **1996**, *77*, 3865–3868. [[CrossRef](#)]
39. Delley, B. Hardness Conserving Semilocal Pseudopotentials. *Phys. Rev. B Condens. Matter Mater. Phys.* **2002**, *66*, 155125–155133. [[CrossRef](#)]
40. Hoheisel, M.; Speller, S.; Kuntze, J.; Atrei, A.; Bardi, U.; Heiland, W. Structure of Pt₃Sn(110) Studied by Scanning Tunneling Microscopy. *Phys. Rev. B Condens. Matter Mater. Phys.* **2001**, *63*, 245403. [[CrossRef](#)]
41. Monkhorst, H.J.; Pack, J.D. Special Points for Brillouin-Zone Integrations. *Phys. Rev. B* **1976**, *13*, 5188–5192. [[CrossRef](#)]
42. Zhu, H.Y.; Guo, W.Y.; Jiang, R.B.; Zhao, L.M.; Lu, X.Q.; Li, M.; Fu, D.L.; Shan, H.H. Decomposition of Methanthiol on Pt(111): A Density Functional Investigation. *Langmuir* **2010**, *26*, 12017–12025. [[CrossRef](#)]
43. Lu, X.Q.; Deng, Z.G.; Guo, C.; Wang, W.L.; Wei, S.X.; Ng, S.P.; Chen, X.F.; Ding, N.; Guo, W.Y.; Wu, C.M.L. Methanol Oxidation on Pt₃Sn (111) for Direct Methanol Fuel Cells: Methanol Decomposition. *ACS Appl. Mater. Interfaces* **2016**, *8*, 12194–12204. [[CrossRef](#)] [[PubMed](#)]
44. Halgren, T.A.; Lipscomb, W.N. The Synchronous-transit Method for Determining Reaction Pathways and Locating Molecular Transition States. *Chem. Phys. Lett.* **1977**, *49*, 225–232. [[CrossRef](#)]

45. Ma, Y.; Hernández, L.; Guadarrama-Pérez, C.; Balbuena, P.B. Ethanol Reforming on Co(0001) Surfaces: A Density Functional Theory Study. *J. Phys. Chem. A* **2012**, *116*, 1409–1416. [[CrossRef](#)] [[PubMed](#)]
46. Jin, Y.X.; Wang, Y.F.; Zhang, R.X. Theoretical Insight into Hydrogen Production from Methanol Steam Reforming on Pt(111). *Mol. Catal.* **2022**, *532*, 112745. [[CrossRef](#)]

Disclaimer/Publisher's Note: The statements, opinions and data contained in all publications are solely those of the individual author(s) and contributor(s) and not of MDPI and/or the editor(s). MDPI and/or the editor(s) disclaim responsibility for any injury to people or property resulting from any ideas, methods, instructions or products referred to in the content.